

Numerical and Experimental Study on Flow Effects of Pneumatic Proportional Pressure Valve

Tzong-Hann Shieh^{*,**}, Chun-Liang Yeh^{*,**}, Yu-Li Chen^{**} and Charng-Chin Hsiao^{**}

Keyword : Pneumatic, Proportional pressure valve, Solenoid valve, Parametric analysis

ABSTRACT

This study developed a novel system for the measurement of pressure within an SMC-ITV2030-012BL pneumatic proportional pressure valves. We also constructed a precise three-dimensional structure of the channel within the valve to examine the aerodynamic characteristics of the internal flow field using the finite volume method and Reynolds-averaged Navier-Stokes equations. We first compared the aerodynamic characteristics resulting from opening the valve 70% using completely or partially encrypted grid models. We then considered various wall structures at the inlet and outlet of the flow channel with the same valve opening. Finally, we compared the results of simulation and experiments of the flow field within the valve. Finally, we investigated the flow field characteristics when the valve was opened 90%, 70%, and 50%. Experiment and simulation results show that the aerodynamic characteristics of the flow field are influenced by the wall structures of the valve and the opening of the valve as well as the grid encryption method that is employed.

INTRODUCTION

Pneumatic actuators are as the primary drive and control components in numerous types of sophisticated machinery, such as that used in manufacturing electronic parts and biomedicine, due to their precision, speed, and level of control.

Paper Received October,2017. Revised August,2019. Accepted August, 2019. Author for Correspondence: Tzong-Hann Shieh

** Department of Aerospace and Systems Engineering, Feng Chia University, 100, Wenhwa Rd., Seatwen, Taichung, Taiwan.*

*** Ph.D. Program of Mechanical and Aeronautical Engineering, Feng Chia University, 100, Wenhwa Rd., Seatwen, Taichung, Taiwan.*

The operation of pneumatic proportional pressure valves involves sending signals to a valve control unit to actuate a solenoid valve and pressure feedback sensor in order to displace the valve and release gas pressure in a proportional manner. Pneumatic actuators were first developed in the 1950s, when Shearer first proposed a dynamic control theory for pneumatic systems. Shearer developed a number of models, to which he applied various types of valve, including on-off solenoid valves and proportional valves (Rahmat et al, 2011). In the late 1960s, the Swiss company Beringer launched KL proportion combination valves, and in 1970 the Japanese company Yuken followed with proportional valve technologies that focus on flow rate and pressure. This established the importance of proportional valve technologies (Lu et al, 1988). In 1983, Schwenzer (1983) used a torque motor and a nozzle-flapper system to adjust the spool position of hydraulic servo valves. In 1986, Moore (1986) designed a direct actuated valve with a proportional valve and no internal feedback loop. By 1990, the engagement of major manufacturers around the world, the continuing development of the control theory, and system integration techniques for proportion components made it possible to integrate sensors, proportional-integral-derivative (PID) controllers, and other components in highly functional and reliable proportional valve products. In 1991, Johnston et al. (1991) performed valve flow visualization for a Reynolds number greater than 2,500 under steady flow and non-cavitating conditions. In 1996, Huang et al. (1996) conducted 3D simulation to enable the analysis of butterfly valves using FLUENT software. In 1997, Lee et al. (1997) used the finite element method, the Newmark approach, and steady incompressible fluid conditions to investigate transient fluid-structure interactions in valves.

In 1999, Araki et al. (1999) performed experiments to determine the influence of key parameters on the performance of diaphragm-type proportional pressure relief valves, which led to the

construction of a relevant mathematical model. In 2000, Richer et al (2000) used dual action pneumatic actuators in the development of a mathematical model for the control of proportional valves. In 2002, James et al (2002) used computational fluid dynamics (CFD) simulation software in conjunction with the Reynolds function to calculate the overall flow coefficient and the relative valve capacity factor of globe control valves. They also presented simplified geometric models with a large range of valve openings with which to conduct 3D simulations followed by experimental verification. In 2004, Sorli et al. (2001, 2004) investigated pneumatic proportional valves (EPP3 J-21-U-100-10 from Lucifer, now Honeywell) under a variety of load conditions to examine the influence of time and frequency on static and dynamic parameters in a nonlinear mathematical model. Figliolini et al. (2004) studied the parameters of SMC-VEF valves under the same conditions. Scholz et al (1992), Zhou (1995), and Jimenez et al (2004) performed detailed analysis on the characteristics of proportional directional control valves in the FESTO-MPYE series. In 2005 and 2006, Fiedler et al (2005) and Cho et al. (2006) analyzed the characteristics of FESTO-MPPES valves. Miyajima et al. (2007) focused on displacement sensors and air bearings in the design of a spool-type proportional valve in 2007 with a maximum response frequency of 300 Hz. In 2011, Cheng et al. (2011) used the Labview program design platform to send valve control signals to a piezoelectric motor through an RS232 interface, obtain pressure sensor feedback via a data acquisition (DAQ) card, and analyze the static and dynamic output characteristics of valve closed loops. In 2012, Cheng et al (2012) developed a setup for pneumatic experiments based on ISO6358 and derived a mathematical model of the dynamic responses of an active pneumatic vibration isolator via experiments and simulations.

Current research has been focused on the simulation of valve control units, the capture of signals and feedback data, and the mathematical modeling of proportional valves. Previous research involving the simulation of flow fields within proportional valves considered only simplified models and captured flow field situations only at the spool. Research into the three-dimensional simulation of the overall aerodynamic field within proportional valves remains inadequate. This study constructed a precise three-dimensional rendering of the channel within an SMC-ITV2030-012BL proportional valve to examine the aerodynamic characteristics of the flow field. To enable a systematic approach, we divided our investigation into three segments. We first calculated the three-dimensional flow fields resulting from coarse and fine grid models when a valve is 70% open. We then considered the characteristics of the flow field resulting from various

internal wall structures at the inlet and outlet of the channel with the valve opened to the same amount (70%) as well as 50% and 90%. Finally, we constructed a new pneumatic measuring system for use in measuring flow pressure within the channel of the proportional valve, and compared the results with those obtained in simulations.

PNEUMATIC PROPORTIONAL PRESSURE VALVES: BASIC PRINCIPLES

As shown in Fig. 1, the principle behind actuating a pneumatic proportional pressure valve consists of four function blocks: a logic program block, a command block, a drive block, and a feedback block. The actuation procedure involves augmenting the input signal of the logic program block to switch open the inlet solenoid valve and reset the outlet solenoid valve to closed. The gas entering the primary inlet of the valve moves into the pilot chamber via the inlet solenoid valve. Increasing the internal pressure creates displacement in the sliding shaft of the valve, thereby opening the valve and achieving output at the target pressure. Furthermore, to ensure that the output pressure as close to the preset target as possible, the primary outlet of the valve is equipped with a pressure feedback sensor to gauge the pressure. The pressure feedback is sent to the control circuit, which repeatedly compares the feedback with the target value and makes adjustments until the pressure output reaches a specific proportion of the input signal. Simultaneous with valve actuation, the feedback signals influence changes in the command signal, which then prompts the desired responses in the internal valve drive, thereby generating the target pressure output.

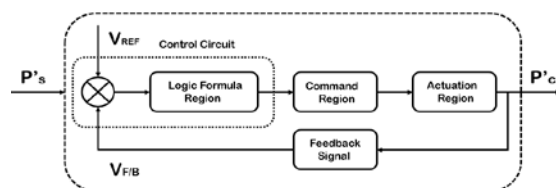


Fig. 1. Principle of pneumatic proportional valve

COMPUTATIONAL AND EXPERIMENTAL METHODS

Simulation methods and Turbulence Model

In dealing with the conservation equations for fluid motion, we incorporated a three-dimensional non-steady Navier-Stokes equation into the test model in order to obtain the velocity, temperature, pressure, and density of the fluid. The Navier-Stokes equation is a partial differential equation used to describe turbulent flow under considerations of

viscosity, thermal conductivity, and the compressibility of the flow field. The conservation laws pertaining to the mass, momentum, and energy of continuous fluid media form the basic conditions (Launder et al, 1972). In practical engineering, the theory of nonlinear partial differential equations is not sufficiently comprehensive to solve the Navier-Stokes equations directly. This requires large-scale vortex simulation and the Reynolds-averaged time simulation. The former employs a non-steady Navier-Stokes equation to simulate the movement of large-scale vortices in conjunction with preset models for use in simulating the movement of small-scale vortices. The latter approach uses Navier-Stokes equations to average time, whereupon models are imported for numerical solution. To reduce computation time, we adopted a pressure-based solver for the calculations used in numerical simulation and paired it with the finite volume method to solve the Reynolds-averaged Navier-Stokes equations shown in Eqs. (1) and (2). For spatial discretization, we adopted the SIMPLE algorithm coupled with pressure and velocity. We used a first-order discretization scheme for the preliminary calculations in order to obtain preliminary solutions of lower accuracy. Once the first-order calculations converged, we used a second-order discretization scheme to increase the accuracy of the solutions.

$$\frac{\partial \rho}{\partial t} + \frac{\partial}{\partial x_i}(\rho u_i) = 0 \quad (1)$$

$$\frac{\partial}{\partial t}(\rho u_i) + \frac{\partial}{\partial x_j}(\rho u_i u_j) = -\frac{\partial p}{\partial x_i} + \frac{\partial}{\partial x_j} \left[\mu \left(\frac{\partial u_i}{\partial x_j} + \frac{\partial u_j}{\partial x_i} - \frac{2}{3} \delta_{ij} \frac{\partial u_k}{\partial x_k} \right) \right] + \frac{\partial}{\partial x_i}(-\rho \overline{u_i u_i}) \quad (2)$$

For the turbulence model, we used a $k-\omega$ SST double-equation model to calculate the solutions based on the principle of Reynolds-averaged time simulation. The standard $k-\omega$ model was modified from the Wilcox $k-\omega$ model to take into account conditions such as low Reynolds numbers, compressibility, and the propagation velocity of shear flow. The $k-\omega$ SST model developed by Menter (1994) is similar to the standard $k-\omega$ model. To enhance the accuracy of calculations in regions near the walls of flow fields, in calculating the viscosity of turbulent flow in the model, we also considered the propagation of shear stress in order to convert the transfer equation into equations of turbulence kinetic energy k equation and dissipation rate ω , as shown in Eqs. (3) and (4), respectively.

$$\frac{\partial}{\partial t}(\rho k) + \frac{\partial}{\partial x_i}(\rho k u_i) = \frac{\partial}{\partial x_j} \left(\Gamma_k \frac{\partial k}{\partial x_j} \right) + \tilde{G}_k - Y_k \quad (3)$$

$$\frac{\partial}{\partial t}(\rho \omega) + \frac{\partial}{\partial x_i}(\rho \omega u_i) = \frac{\partial}{\partial x_j} \left(\Gamma_\omega \frac{\partial \omega}{\partial x_j} \right) + G_\omega - Y_\omega + D_\omega \quad (4)$$

\tilde{G}_k denotes the kinetic energy of turbulence generated by the average velocity gradient; G_ω is the ω equation, and Γ_k and Γ_ω are the terms of effective diffusion in the k and ω equations, respectively; D_ω is the orthogonal dissipation term; Y_k and Y_ω represent the turbulent flow produced through diffusion. Thus, the $k-\omega$ SST model has greater precision and credibility than does the standard $k-\omega$ model in the expansive domain of fluid motion. It is also advantageous in the prediction of turbulence in near-wall regions in avoiding errors pertaining to complex flow calculations in the first-order discretization scheme. This also resolves the problems of long computation time and poor convergence in the second-order discretization scheme. Flow field simulations are used for nonlinear conservation analysis; therefore, under relaxation factors are used in the separated solution approach to ensure that the derived flow field variables are slightly below than the actual calculation values. The equation is shown in Eq. (5).

$$\phi = \phi_{old} + \alpha \Delta \phi \quad (5)$$

In the formula above, ϕ is the actual calculation result, ϕ_{old} is the calculation result of the previous step, α is the calculation result of the previous step, α is the under relaxation factor, and $\Delta \phi$ denotes the increment obtained from the calculations. For most flow field analyses, the under relaxation factor is only decreased when instability or divergence appears during the analysis.

Experimental Setup

To measure the pressure within the channel of the proportional valve, we included a pneumatic flow restrictor that complies with the international ISO6358 standards (Cheng et al, 2012) on which we based the development of a novel pneumatic measurement system. The testing platform includes a high-pressure air supply system (SWAN, HWU-310CN-1,220V/60HZ), a precision pressure regulator (CKD-RP2000), a data acquisition card (NI-6210), a DC power supply (HILA, DP-30052, 30V-5A), and a PLC control system. The setup of the measurement system is presented in Fig. 2

Five pressure sensors (S'mate, 33A 150G 2210) were installed within the valve to measure pressure in the near-wall region. The precision of the pressure sensors was within $\pm 1.8\%$. Figs 3 and 4 exhibit the locations of the sensors and the reference value calibration curve obtained from pressure feedback signals. As shown in Fig. 3, measurement points 1 and 5 are located in the structural spaces remaining from where the inlet and outlet connectors are linked to the valve, respectively. Measurement point 3 is situated in the space of the sliding shaft and the movable slide structure, and measurement points 2

and 4 are at the entrances of the inlet solenoid valve and the pressure feedback sensor. As shown in Fig. 4, the reference value of the calibration curve obtained from the pressure feedback signals was derived from air pressure values between 0.5 bar and 5.5 bar and voltage values. The intervals between the tested pressure values was 0.5 bar, and the value capture frequency was 1,000 times/sec. Pressure values measured in the near-wall region served as the basis of comparison with the simulation results.

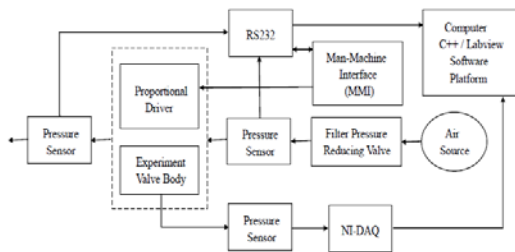
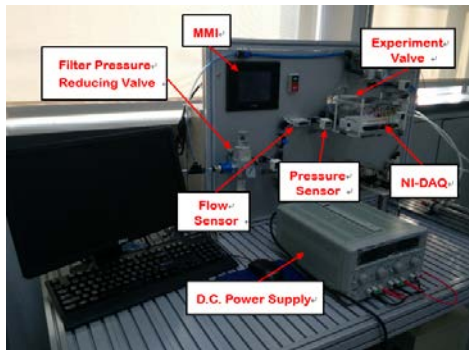


Fig. 2. Experimental platforms

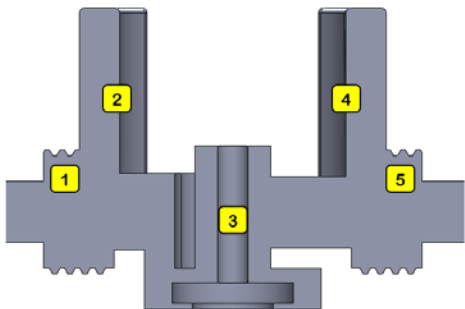


Fig. 3. Measurement point of pressure sensor

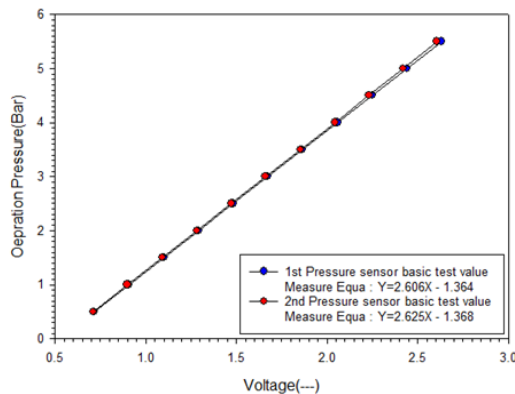


Fig. 4. Regulate curve of pressure sensor
PHYSICAL MODEL, GRIDS, AND

BOUNDARY CONDITIONS

To evaluate the valve structure, we considered the SMC-ITV2030-012BL proportional valve series. Figure 5 presents a three-dimensional rendering of the structure of the valve.

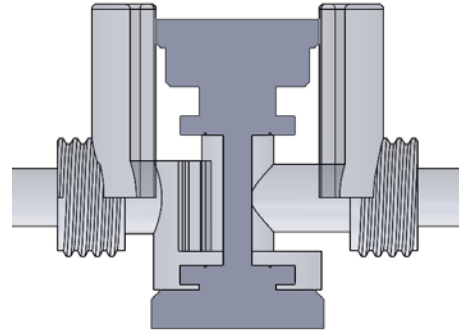


Fig. 5. 3D structure of SMC ITV-2030 valve

In the design of the grid, we used a three-dimensional configuration combining coarse and fine grids to adjust and encrypt the overall grid and boundary layer grids of the flow field. To illustrate the grid design, the area of the green dashed line in Fig.6-a (70% opening degree of valve, w. screw threads) is magnified in Figs. 6-b through 6-d. Fig. 6-b displays a basic configuration with 1.2 million grids. Subsequent encryption of the overall grid and boundary layer grids of the flow field were based on this grid design. Distances to the wall were non-dimensionalized to design the boundary layer grids near the walls in conjunction with preset parameters such as free flow velocity, free flow density, the dynamic viscosity coefficient, and the inlet pipe diameter. The non-dimensionalization of the distance to the wall was performed using Eq. (6).

$$y^+ \equiv (u * y) / \nu \tag{6}$$

In the above formula, u is the near-wall friction velocity, y denotes the distance to the boundary layer formed by the walls, and ν is the dynamic viscosity coefficient of the local fluid. Accordingly, gridding of the near-wall boundary layer was further divided into two situations using the y^+ equation above, with y^+ ranging from 1 to 2. Under such circumstances, we established two configurations with different grid densities, as shown in Figs. 6-c and 6-d.

To speed up calculations and reduce simulation time, we adopted a mix of hexahedron structure grids and tetrahedron grids at the primary inlet and outlet of the valve, the entrance of the inlet solenoid valve, and the inlet channel of the pressure feedback sensor. In addition, we used pyramid-shaped pentahedron grids between the tetrahedron grids and the tri-prism pentahedron grids.

With regard to the boundary conditions, the fluids within fluid mechanical components are generally non-steady when a device is turned on or

off; once the device has been running for a certain period of time, the fluids reach a steady state and are then regarded as a steady flow. The simulation environment established in this study involved the valve being operated in conditions of steady flow. The measurements at the primary inlet and outlet of the valve serve as the initial conditions of the flow field aerodynamics within the valve. At room temperature, the free flow pressure is approximately 570 kPa, whereas the free flow velocity is roughly 200 m/s.

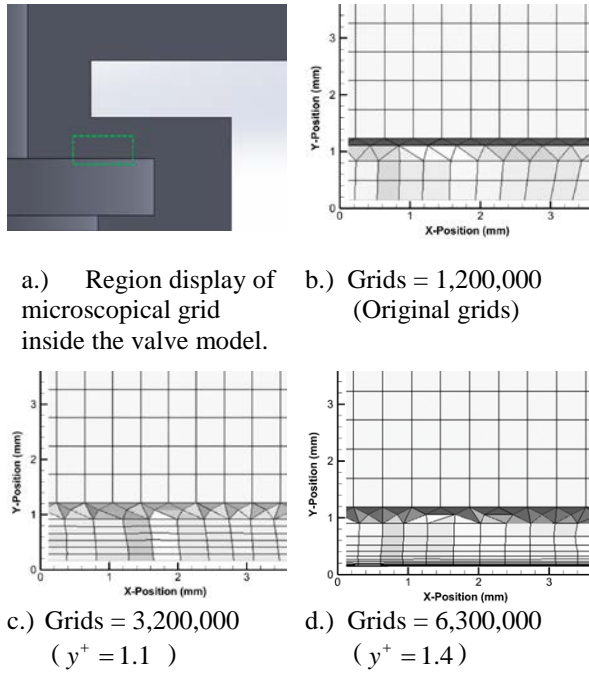


Fig. 6. Microscopical grid of numerical model

RESULTS AND DISCUSSION

Encryption Methods Used in Grid Models

This section deals with the three-dimensional structure of a pneumatic proportional pressure valve and grid designs of various densities. We first examined how the encryption of the entire flow field grid and the boundary layer regions influence the aerodynamic characteristics of the internal flow field. The results are shown in Figs. 7 through 11. Fig. 7 displays the actual locations of the near-wall pressure values extracted from the calculation results of the three-dimensional flow field in the valve. The locations are identical to the five points at which pressure was measured in the experiment, as shown in Fig. 5. Figs 8 and 9 present the calculation results for a valve opening of 70% for basic gridding using 1.2 million grids and the completely encrypted grids with 4 million and 7.3 million grids, respectively. As shown in Fig. 8, the distribution of pressure near the walls does not differ significantly from that measured in the experiment. This demonstrates that encrypting the overall grid did not enhance the precision of

near-wall pressure calculations. Thus, we used the percentages of error between the simulations and the experiments to determine the standard deviation in the pressure measurements and evaluate the precision of the encryption designs. The figure shows that the error percentages of all encrypted grid designs fell outside the standard deviation of the experiment values, ranging from 8% to 13%.

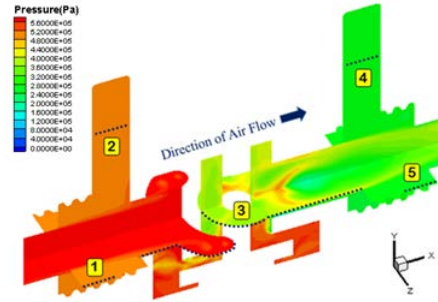


Fig. 7. Data line on flow field of pressure measurement point

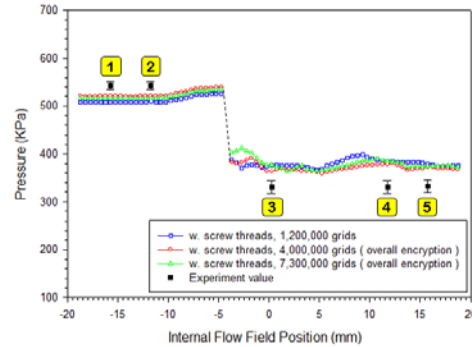


Fig. 8. Distributions of the near-wall pressure with different density grid models (70% opening degree of valve, w. screw threads, Overall encryption grids)

To overcome this problem, we performed partial encryption, encrypting only the boundary layer grids near the walls. In other words, we constructed two other partially encrypted grids with 3.2 million and 6.3 million grids based on the grid design with 1.2 million grids and the same valve opening. The calculation results are displayed in Figs. 10 and 11. Fig. 10 shows that the simulation values at pressure measurement points 1 and 2 are still lower than the experiment values. The cause of this is the turbulence model, which overestimated the flow field resistance in the boundary layer at the valve inlet and thus underestimated the pressure. The discrepancy was approximately 50 kPa. For the most part, the encrypted grid design with 6.3 million grids presented near-wall pressure distributions that were closer to the experiment measurements than those obtained from the grid designs with 1.2 million grids and 3.2 million grids. Fig. 11 compares the standard deviations in the experiment pressure measurements in the partially encrypted grid designs. As can be seen, the percentages of error between the simulations and experiments based on the encrypted grid design with

6.3 million grids all fall within the standard deviation of the experiment values, ranging from 3% to 6%. This indicates that this design displays sufficient calculation precision.

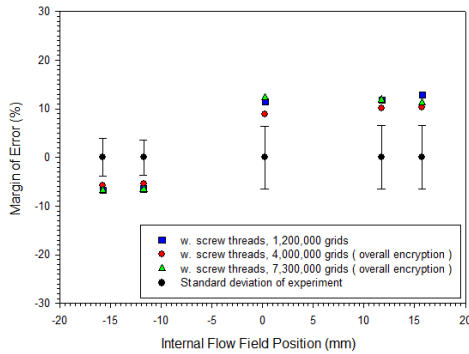


Fig. 9. Experimental standard deviation data compare with margin of error in simulation and experiment (70% opening degree of valve, w. screw threads, Overall encryption grids)

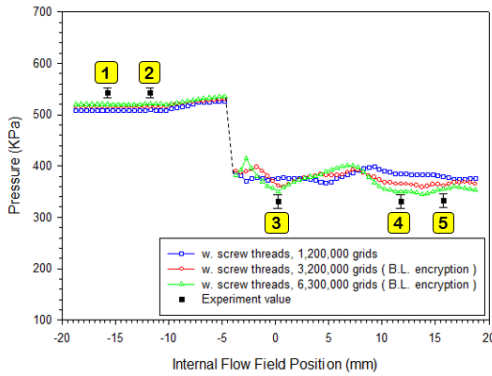


Fig. 10. Distributions of the near-wall pressure with different density grid models (70% opening degree of valve, w. screw threads)

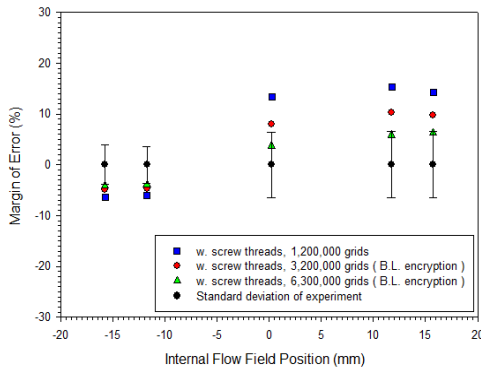


Fig. 11. Experimental standard deviation data compare with margin of error in simulation and experiment (70% opening degree of valve, w. screw threads)

Geometry Structure with and without Screw Threads

In this section, we examine the influence of internal wall structures on the aerodynamic characteristics of the flow field. Based on the results in section for “Encryption Methods Used in Grid

Models” and in view of the overly long computation time, we adopted a flow field model with encrypted boundary layer grids to accelerate convergence. We first examined models with and without threaded wall structures at the valve inlet with the valve 70% open. Using the grid design with 1.2 million grids, we performed partial encryption and created an integrated grid with 6.3 million grids. The definition of local and the calculation results are presented in Figs. 12 through 16. The calculated area of the flow field was based on Fig. 12, in which the green dashed line shows where the analysis of aerodynamic characteristics is particularly focused. The red dashed line indicates the changes in wall structure, and the yellow dashed lines circle the spool outlet and the inlet of the pressure feedback sensor.

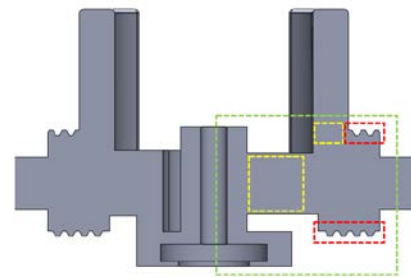


Fig. 12. Region display of streamline and pressure isosurface inside the valve flow-field (70% opening degree of valve, w. screw threads)

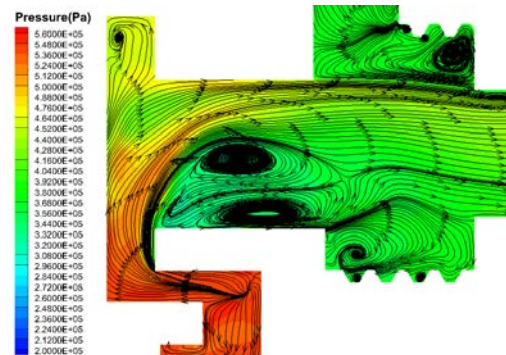


Fig. 13. Streamline and pressure isosurface inside the valve flow-field (70% opening degree of valve, w. screw threads)

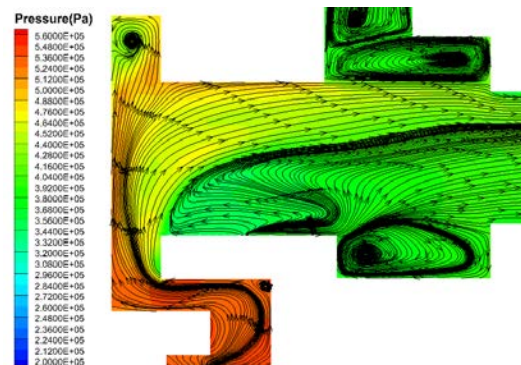


Fig. 14. Streamline and pressure isosurface inside the valve flow-field (70% opening degree of valve, w.o. screw threads)

Figs 13 and 14 respectively show the flow lines and pressure isosurfaces in the flow field with and without threaded wall structures. A comparison of the results indicates that vortex generated near the spool outlet was strengthened by the threaded wall structure, which indirectly influenced the distribution of vortices in the channel inlet of pressure feedback sensor. Fig. 15 displays the changes in near-wall pressure at the inlet and outlet of the flow channel in situations with and without the threaded wall structures. As can be seen in the figure, the presence of the threaded wall structures did not produce significant differences in the simulated near-wall pressure values at measurement points 1 or 2. With threaded wall structures, the experimental and simulated near-wall pressure values at measurement points 3, 4, and 5 were more consistent. Furthermore, the simulated near-wall pressure values without threaded wall structures were higher than those with threaded wall structures, which is because the threaded wall structures greatly affect the distribution of vortices in the flow field. The more widespread the vortex structure enhancement is, the greater the extent of pressure loss is. This reduces the pressure values in the flow channel, as verified by the isosurfaces in Figs. 13 and 14.

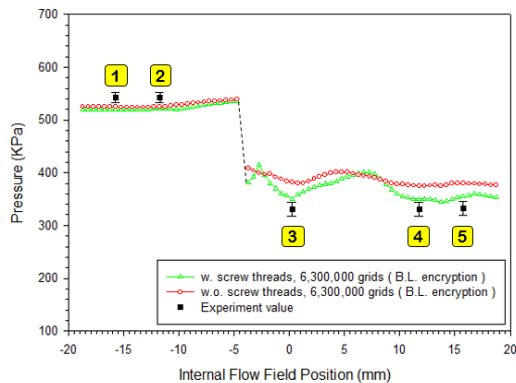


Fig. 15. Distributions of the near-wall pressure with different wall structures (70% opening degree of valve, w. screw threads and w.o. screw threads)

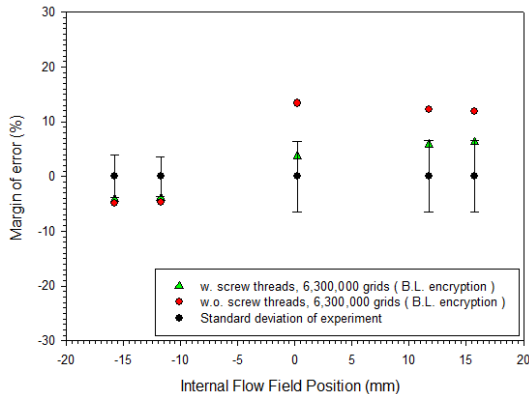


Fig. 16. Experimental standard deviation data compare with margin of error in simulation and experiment (70% opening degree of valve, w. screw threads and w.o. screw threads)

Fig. 16 compares the standard deviations in the experiment and the percentages of error between simulated and experiment values with and without threaded wall structures. As can be seen, situation with no threaded wall structures at the inlet or outlet of the flow channel resulted in the error percentages at all pressure measurement points falling outside the experimental standard deviation, ranging from 12% to 15%. In contrast, with threaded wall structures at the inlet and outlet of the flow channel, the error percentages of all pressure measurement points fell within the experimental standard deviation, dropping significantly from between 12% and 15% to between 3% and 6%.

Variations in Valve Opening

Based on the simulation conditions in first and second Sections, the results in this section are divided into two parts. The first part examines how the degree to which the valve is opened affects the flow field characteristics, using valve openings of 90%, 70%, and 50%. Figs 17 through 19 present the flow lines and pressure distributions within the valve. As can be seen, after the gas enters the channel inlet but before it reaches the valve structure, vortices are produced near the entrance of the inlet solenoid valve and in the structural space where the inlet connector is linked to the valve. As a result, the channel pressure is reduced to approximately between 520 kPa and 540 kPa. Once the gas enters the moving chamber of the sliding shaft, vortex flows are also produced near the outlet valve port, which gradually decrease the pressure within the channel. Furthermore, when the gas reaches the outlet region of the channel, vortices are also produced in the space where the outlet connector is linked to the valve. This vortex flow produces a saddle point in the flow field above the threaded wall structures, which creates a dead zone. In addition, it decreases the pressure in the outlet region of the valve channel. As the opening percentage of the valve decreases from 90% to 50%, the vortex structures near the inlets of the pressure feedback sensor and the moving chamber of the sliding shaft expand, which promotes a significant pressure drop from between 460 kPa and 480 kPa to between 260 kPa and 300 kPa.

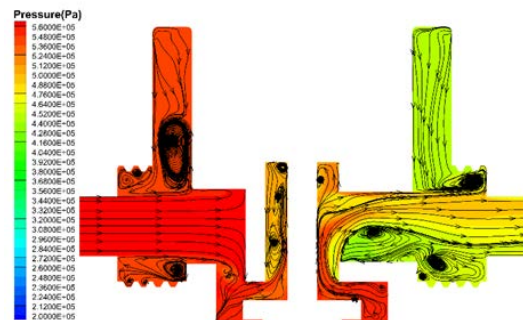


Fig. 17. Streamline and pressure isosurface inside the valve flow-field (90% opening degree of valve, w. screw threads)

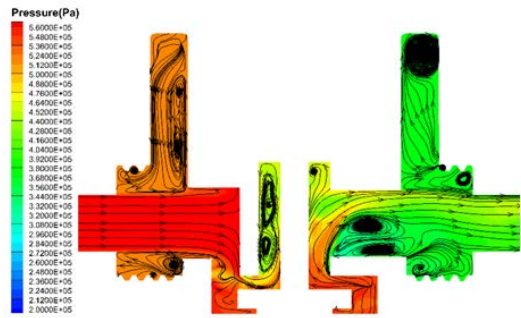


Fig. 18. Streamline and pressure isosurface inside the valve flow-field (70% opening degree of valve, w. screw threads)

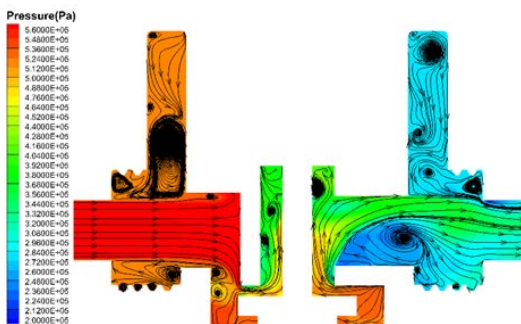


Fig. 19. Streamline and pressure isosurface inside the valve flow-field (50% opening degree of valve, w. screw threads)

In the second part of the experiment, we examined the characteristics of the flow field near the valve inlet, as shown in Fig. 20 (green dashed line/near moving chamber of sliding shaft). Figs 21 through 23 displays the flow lines and pressure isosurfaces near the valve inlet with the valve opened 90%, 70%, and 50%, respectively.

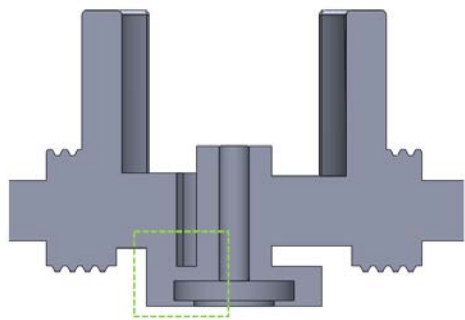


Fig. 20. Region display of streamline and pressure isosurface inside the valve flow-field (70% opening degree of valve, w. screw threads)

As can be seen, when the gas enters the valve inlet, the formation of a saddle point promotes the initial formation of vortexes in this flow region (such as Location 1 in Fig. 21). Next, when the opening of the valve is reduced from 90% to 70%, the saddle point moves downstream with the gradually increase in flow velocity and decrease in sectional area of the channel, resulting in more distinct vortex flows (such as Location 2 in Fig. 22). When the valve opening

was decreased from 70% to 50%, the saddle point migrated toward the left wall to forms a clear, solid vortex structure, creating secondary flows. The development of this vortex structure is a result of the overall pipeline or circuit passing a valve or bend, which forms obstacles to the originally smooth flow and results in secondary energy loss and a further drop in pressure. This is because the gas is flowing from a wider channel to a narrower channel, which creates an irreversible pressure head loss at the connection.

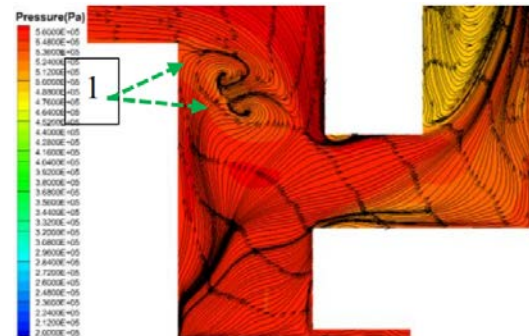


Fig. 21. Streamline and pressure isosurface inside the valve part flow-field of inlet (90% opening degree of valve, w. screw threads)

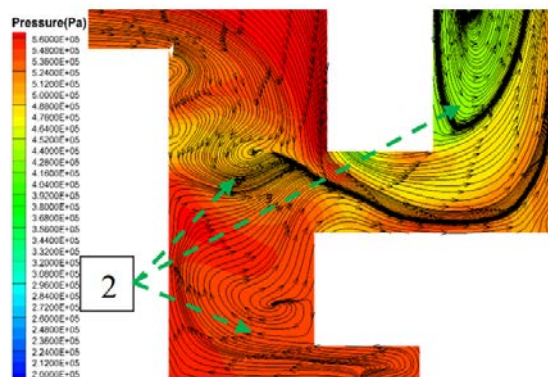


Fig. 22. Streamline and pressure isosurface inside the valve part flow-field of inlet (70% opening degree of valve, w. screw threads)

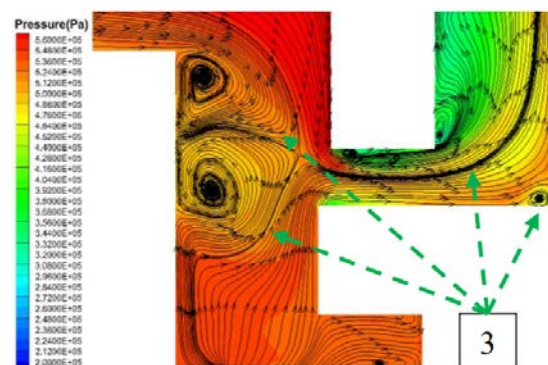


Fig. 23. Streamline and pressure isosurface inside the valve part flow-field of inlet (50% opening degree of valve, w. screw threads)

The pressure head loss is also influenced directly by the bend in the channel; a ninety-degree bend

creates a sharper impact on the flow, causing the velocity and pressure heads to separate and generating vortices, which produces what is known as secondary flow. This further constricts the channel, increasing the flow velocity and reducing the pressure slightly. In this region of the channel, this flow process creates unnecessary airflow resistance, which then impacts the aerodynamic characteristics of the flow field at the valve inlet.

CONCLUSIONS

This study constructed a novel system to measure the pressure within SMC-ITV2030-012BL pneumatic proportional pressure valves. We also constructed a precise three-dimensional structure of the channel within the valve and examined the aerodynamic characteristics of the internal flow field. The results of this study are divided into three parts.

In the first part, with a valve open 70% and a completely encrypted flow field grid, the calculated near-wall pressure distributions showed no significant differences from measurements obtained in experiments. The error percentages of all the encrypted grid designs fell outside the standard deviation of the experiment values, ranging from 8% to 13%. Among the partially encrypted grids in which only the boundary layer grids were encrypted, the percentages of error between the simulations and experiments based on the encrypted grid design with 6.3 million grids all fell within the standard deviation of experiment values, ranging from 3% to 6%. This indicates that this design displays sufficient calculation precision.

In the second part, with a valve opening of 70% and a partially encrypted grid, the results showed that the vortex structures generated near the valve outlet are strengthened by threaded wall structures, which indirectly influences the distribution of vortices at the inlet of the pressure feedback sensor. In the case without threaded wall structures at the inlet or outlet of the flow channel, the error percentages of all the pressure measurement points fell outside the experimental standard deviation, ranging from 12% to 15%. In contrast, in the case with threaded wall structures at the inlet and outlet of the flow channel, the error percentages of all the pressure measurement points fell within the experimental standard deviation, dropping significantly to between 3% and 6%. These results demonstrate that threaded wall structures at the inlet and outlet of the flow channel have a degree of influence on the flow field within the valve.

The third part investigated situations in which the valve was opened 90%, 70%, and 50% using partially encrypted grids. The results showed that as the valve opening is reduced, the saddle point produced in this flow region moves downstream with the gradually increase in flow velocity and decrease in sectional area of the channel, which produced more distinct vortex structures and secondary flows. This forms

obstacles in the originally smooth flows and results in secondary energy loss and a further drop in pressure, which produces unnecessary resistance to airflow.

ACKNOWLEDGEMENTS

This study was supported by the Ministry of Science and Technology (MOST108-2221-E-035-023-MY3 & MOST107-2221-E-035-043-MY2), and was completed due to the support of Mr. Ping-Cheng Yu, we want to thank for the valuable help cordially.

REFERENCE

- Rahmat, M.F., Sumar, N.H., Salim, S. N.S., Abidin, M. S.Z., Fauzi, A.A.M. and Ismail, Z.H., "Review on Modeling and Controller Design in Pneumatic Actuator Control System", *International Journal on Smart Sensing and Intelligent Systems*, vol., 4, no. 4, pp. 630-661. (2011).
- Lu, Y.S. Lu and Hu D.H., "Electrical liquid proportional control technology", Beijing, Mechanical industry publishing house. (1988).
- Schwenzer, R., "Entwurf und Auslegung servopneumatischer Antriebsregelungen", Diss., RWTH Aachen. (1983).
- Moore, P.R., "Pneumatic motion control systems for modular robots", Ph.D. thesis, Uni. of Loughborough. (1986).
- Johnston, D.N., Edge, K.A., and Vaughan, N.D., "Experimental Investigation of Flow and Force Characteristics of Hydraulic Poppet and Disc Valves", *Proc. Inst. Mech. Eng.*, 205, pp. 161-171. (1991).
- Huang, C., and Kim, R.H., "Three-Dimensional Analysis of Partially Open Butterfly Valve Flows", *ASME J. Fluids Eng.*, 118, pp. 562-568. (1996).
- Lee, J.J., and Wellford, L.C., "Transient Fluid-Structure Interaction in a Control Valve", *ASME J. Fluids Eng.*, 119, pp. 354-359. (1997).
- Richer, E. and Hurmuzlu, Y., "A high performance pneumatic force actuator system. Part 1 - Nonlinear mathematical model", *Trans ASME, Journal of Dynamic Systems, Measurement, and Control* 122(3): 416-425, (2000).
- James, A.D. and Mike, S., "Predicting Globe Control Valve Performance-Part I: CFD Modeling", *ASME Trans. Journal of Fluids Engineering*, vol. 124, pp. 772-777, Sept. (2002).
- James, A.D. and Mike, S., "Predicting Globe Control Valve Performance-Part II - Experimental Verification", *ASME Trans. Journal of Fluids Engineering*, vol. 124, pp. 778-783, Sept. (2002).
- Sorli M., Figliolini G. and Pastorelli S., "Dynamic Model of a Pneumatic Proportional Pressure Valve", *IEEE/ASME International Conf.*

- Advanced Intelligent Mechatronics Proceedings, Como, Italy, 8-12 July (2001).
- Sorli, M., Figliolini, G. and Pastorelli S., "Dynamic Model and Experimental Investigation of a Pneumatic Proportional Pressure Valve," IEEE/ASME Trans. Mechatron., vol. 9, no. 1, pp. 78-86, (2004).
- Figliolini, G., Almondo, A. and Sorli, M., "Modelling and experimental validation of a pneumatic servo-solenoid valve", Proc. Power Transmission and Motion Control PTMC, Bath, pp 85-98, (2004).
- Scholz, D. and Schwenzer, R., "Schnelles pneumatisches Proportionalventil mit integrierter Elektronik fuer die breite Anwendung", Proc 10. Aachener Fluidtechnisches Kolloquium, Aachen, pp 129-140, (1992).
- Zhou, H., "Intelligence in pneumatic servo positioning axis", Proc. 4th Scandinavian Int. Conf. on Fluid Power, Tampere, pp. 556-568, (1995).
- Jimenez, A.F. and Garcia, J.P., "Compressible bench flow adaptations to the experimental characterization of pneumatic components. Application to the determination of flow-rate characteristics of a Festo MPYE-5-3/8-010-B proportional valve", Proc 3rd FPNI Ph.D. Symp, Terrassa, (2004).
- Fiedler, M., Helduser, S. and Rudiger, F., "Virtual design of high dynamic pneumatic valves", Proc Power Transmission and Motion Control PTMC, Bath, pp.255-265. (2005).
- Cho, S., Fiedler, M., Rudiger, F. and Helduser, S., "Virtual-design-model-based pressure-tracking control of high-dynamic pneumatic valves using a sliding modecontroller combined with a proportional-integral-derivative scheme.", Proc. Instn. Mech. Engrs. - Part I Journal of Systems and Control Engineering 220(5): 353-365, (2006).
- Cheng, T.H., Gao, H., Bao, G. and Huang, Y., "Realization of Testing System for Electro-Pneumatic Proportional Pressure Valve Based on Virtual Instrument", Singapore. WCSE 2011: 14-16 October (2011).
- Cheng, C.Y. and Renn, J.C., "Modeling and Experiment of an Active Pneumatic Vibration Isolator According to ISO 6358", Journal of the Chinese Society of Mechanical Engineers, vol.33, no.1, pp.51-57, (2012).
- Lauder, B.E and Spalding, D.B., "Lectures in mathematical models of turbulence academic press", London, (1972).
- Menter, F.R., "Two-equation eddy-viscosity turbulence models for engineering applications", AIAA Journal, Vol. 32, No. 8, pp. 1598-1605, (1994).
- Araki, K., Chen, N., "Pressure versus Flow Characteristics of a Diaphragm Type Pneumatic Pressure Control Proportional Valve". Proc. of the 4th JHPS Int. Sym. on Fluid Power, Tokyo, Japan, pp. 413-418. (1999).
- Miyajima, T., Fujiata, T. Sakaki, K., Kawashima, K. and Kagawa, T., "Development of a Digital Control System for High-Performance Pneumatic Servo Valve", Precision Engineering, 31(2), pp. 156-161. (2007).

氣動式比例壓力閥流場特性計算與實驗研究

謝宗翰 葉俊良 陳勇廷 蕭長鑫

逢甲大學航太與系統工程學系

逢甲大學機械與航空工程博士學位學程

摘要

本文採用新建構之氣動式量測系統，針對 SMC-ITV2030-012BL 氣動式比例壓力閥內部流道進行壓力量測實驗。此外，建構出該受測比例閥整體流道之精確三維幾何結構模型，並使用有限體積法，以雷諾平均求解 Navier-Stokes 方程，進行閥體內部流場特性之詳細計算與分析。本研究首先，針對 70% 閥口開度，透過流場網格整體加密與邊界層區域性網格加密兩種不同網格模型配置方式，進行流場氣動力參數特性之模擬與比較分析。其次，針對同一閥口開度，進一步考慮流道出入口處不同壁面幾何結構，進行閥體內部流道之三維流場計算模擬並與實驗結果進行比較。最後，將針對 90%、70% 與 50% 等三種不同閥口開度條件，進行流場變化的動態特性分析。由實驗與計算結果可知，流場邊界層網格、閥體壁面幾何結構和閥口開口比率的改變，均會對閥體結構的流場氣動力特性產生一定程度的影響。